JOURNAL OF GEOPHYSICAL RESEARCH, VOL. 112, D14303, doi:10.1029/2006JD007625, 2007

One-dimensional variational retrieval of aerosol extinction coefficient from synthetic LIDAR and radiometric measurements

N. Huneeus[1] and O. Boucher[2]

Received 6 June 2006; revised 26 December 2006; accepted 8 February 2007; published 19 July 2007.

[1] The Cloud and Aerosol Lidar with Orthogonal Polarization (CALIOP) [onboard the Cloud-Aerosol Lidar and Infrared Pathfinder Satellite Observations (CALIPSO) platform] and the Moderate Resolution Imaging Spectroradiometer (MODIS) instrument (onboard the AQUA platform) will provide simultaneous measurements as part of the "AQUA-train," thus offering a unique opportunity to improve our knowledge on aerosol properties and their spatial distribution. Here we investigate to which extent both the vertical distribution of the aerosol extinction coefficient and the aerosol bimodal size distribution can be retrieved from a synergetic use of the vertically-resolved lidar signal and the spectral radiance measurements. To this effect, a variational retrieval scheme based on a simplified radiative transfer model was developed. The extinction-coefficient profile for fine and coarse-mode aerosols was retrieved from synthetic observations of the profile of the attenuated backscatter lidar signal at two wavelengths and radiances at six wavelengths. Our method aims at minimizing a cost function which measures the departure of the solution to the observations. The adjoint method was applied to find the gradient of the cost function with respect to the input parameters. The retrieval scheme was tested under a realistic noise level and different microphysical perturbations. The retrieval of extinction-coefficient profiles, for fine and coarse particles, is successful if there is a predominance of fine particles. If coarse particles dominate over fine ones, the scheme retrieves the profile of the total extinction coefficient with a higher confidence than that of the fine mode. When perturbations on the aerosol microphysical properties are introduced, thus simulating a more challenging case with incomplete information of the aerosol model present in the atmosphere, the scheme shows a very good performance in terms of total extinction-coefficient retrieval but less success for individual modes. It retrieves the modal radii for both modes simultaneously but can not retrieve at the same time the refractive index and true-mode radii for both modes. Results also reveal that there is some prospect for improvement in the quality of the retrieval by either increasing the size of the predefined set of aerosol models or by including other sources of independent information such as Polarization and Directionality of Earth Reflectances (POLDER)-like measurements.

Citation: Huneeus, N., and O. Boucher (2007), One-dimensional variational retrieval of aerosol extinction coefficient from synthetic LIDAR and radiometric measurements, *J. Geophys. Res.*, *112*, D14303, doi:10.1029/2006JD007625.

1. Introduction

[2] The modeling of present-day climate forcing by aerosol has been mainly approached by means of chemical transport models (CTMs) and general circulation models (GCMs) [e.g., *Collins et al.*, 2001; *Reddy et al.*, 2005]. These models include a representation of aerosols aimed at simulating the three-dimensional distribution of their physical and chemical properties such as concentration, size distribution, chemical composition, and state of mixture. However, it has been recently shown possible to estimate the aerosol direct radiative forcing from satellite observations only [*Bellouin et al.*, 2005; *Kaufman et al.*, 2005; *Yu et al.*, 2006]. Such estimates are nevertheless accurate only for clear-sky conditions. Estimates of all-sky aerosol direct-radiative forcing, as well as the aerosol-indirect effects, depend critically on the aerosol vertical distribution. This is particularly the case for black carbon, which can perturb the temperature profile and thus alter regional circulation and the hydrological cycle [*Ackerman et al.*, 2000; *Menon et al.*, 2002]. The relative importance of the aerosol fine and

[1] Laboratoire d'Optique Atmosphérique, Centre National de la Recherche Scientifique/Université des Sciences et Technologies de Lille, Villeneuve d'Ascq, France.
[2] Hadley Centre, Met Office, Exeter, United Kingdom.

0148-0227/07/2006JD007625$09.00

coarse modes also matters. Fine particles can reduce cloud-droplet size, increase cloud reflectance, and reduce precipitation [*Rosenfeld*, 2000], whereas coarse particles can counteract some of these effects by allowing precipitation and by cleaning the atmosphere of fine particles [*Rosenfeld et al.*, 2002].

[3] When calculating the aerosol radiative impact, both their vertical distribution and the split between fine and coarse particles are therefore important factors. Both these factors can now be addressed in a coherent manner thanks to important progresses made in the clear-sky observation of aerosols from space. Global daily satellite measurements allow retrieving optical thickness and Angström exponent (a signature of aerosol size) from polarized and directional measurements [*Deuzé et al.*, 2000, 2001]. Radiometric measurements from the Moderate Resolution Imaging Spectroradiometer (MODIS) permit to retrieve, among other relevant parameters, aerosol optical thickness and fine-mode fraction based on seven channels with wavelengths in the range from 0.47 to 2.13 μm [*Remer et al.*, 2005]. Measurements with light-detection and ranging (lidar) systems have proven to deliver information on the vertical distribution of aerosols [e.g., *Stephens et al.*, 2001; *Müller et al.*, 2001; *Chazette*, 2003]. The Cloud and Aerosol Lidar with Orthogonal Polarization (CALIOP) instrument onboard the Cloud-Aerosol Lidar and Infrared Pathfinder Satellite Observations (CALIPSO), launched in April 2006, provides profiles of attenuated backscattering coefficients of aerosol and clouds at 0.53 and 1.06 μm. It flies in formation with the Aqua satellite with MODIS onboard and the Polarization and Anisotropy of Reflectances for Atmospheric Sciences coupled with Observations from a Lidar (PARASOL) satellite with a Polarization and Directionality of Earth Reflectances (POLDER)-like instrument onboard. All these instruments allow to observe the same spot on ground with only a few minutes difference. Simultaneous lidar and radiometric measurements will generate data sets that can be used to combine information on the vertical distribution of aerosols from CALIOP and the detailed size information from MODIS and POLDER [*Kaufman et al.*, 2003; *Anderson et al.*, 2005].

[4] Some exploratory studies on the inversion of aerosol fine- and coarse-mode profiles from the synergy of lidar and radiometric measurements have already been conducted [*Kaufman et al.*, 2003; *Léon et al.*, 2003]. They showed the ability to further improve the retrieval of aerosol properties by the combination of active and passive measurements using case studies with lidar measurements taken from an aircraft during different field campaigns. *Kaufman et al.* [2003] showed that the ambiguity in the inversion of the lidar data at two wavelengths can be removed using the MODIS spectral radiances as long as the solution lies within a small set of predefined aerosol models. According to their results, the inversion is robust with respect to noise in the lidar signal but more sensitive to possible calibration errors, although they also argue that the calibration error could be corrected if the aerosol model is known.

[5] Our study explores lidar-radiometer retrievals and revisits some of the conclusions of *Kaufman et al.* [2003] using a variational approach where a cost function is defined and minimized iteratively. The advantages of the method are that it is mathematically rigorous, it takes full account of observational and model errors, and it is easy to include extra constraints and observations. Our method bears some resemblance to that of *Stephens et al.* [2001], who used a nonlinear optimal estimation algorithm to solve the lidar equation [*Marks and Rodgers*, 1993]. Here we use a one-dimensional variational (Var) technique and an adjoint to solve the lidar and radiometer equations. Adjoint methods are powerful modeling tools that allow solving a variety of problems in an efficient way. They are, for instance, used in three-dimensional-Var or four-dimensional-Var data assimilation in order to determine efficiently the optimal initial conditions and also in sensitivity studies to examine the sensitivity of all input parameters with respect to one output parameter [e.g., *Janiskova and Morcrette*, 2005]. Adjoint models allow the computation of the gradient of one output parameter with respect to all input parameters through one single integration, in contrast to the more standard approach of repeatedly integrating the direct model to obtain the sensitivity of all output parameters to perturbations in the input parameters [*Le Dimet and Talagrand*, 1986]. It is our expectation that our method will then feed into variational-data assimilation of aerosol information in three-dimensional atmospheric models.

[6] In this study, we retrieve the extinction-coefficient profile and average size distribution of the fine- and coarse-aerosol modes from synthetic lidar and radiometric measurements. We explore the quality of the solution under different conditions of retrieval. The paper is organized as follows: the inverse problem is presented together with the retrieval scheme in section 2, followed by the presentation of the methodology of our experiments in section 2.5. We present the results in section 3 and the conclusions in section 4.

2. Methodology

[7] The retrieval mechanism is described in detail in this section and is presented schematically in Figure 1. It includes the simplified radiative transfer model described in section 2.2, the calculation of the cost function and its gradient (section 2.1) through the adjoint model (section 2.2), and an optimization routine (section 2.1) that allows the minimization of the cost function. The optimization of the aerosol extinction coefficient and aerosol model is done sequentially rather than simultaneously, with the former being done with a variational approach and the latter in a discrete manner (section 2.5). The retrieval of the aerosol extinction coefficient is repeatedly performed for a set of predefined aerosol models; we retain as solution(s) the retrieval with the smallest residual cost function(s). The predefined aerosol models are presented in section 2.3.

2.1. Variational Retrieval

[8] The goal of variational retrieval is to seek an optimal balance between the observations and a priori information. The departure of a potential solution x to a given observation vector, y^{o}, and to an a priori, x^{b}, is expressed by a scalar function, namely the cost function, and defined as follows:

$$J(x) = \frac{1}{2}\left(x - x^{b}\right)^{T}\mathbf{B}^{-1}\left(x - x^{b}\right) + \frac{1}{2}\left(y^{o} - \mathbf{H}[x]\right)^{T}\mathbf{R}^{-1}\left(y^{o} - \mathbf{H}[x]\right) \quad (1)$$

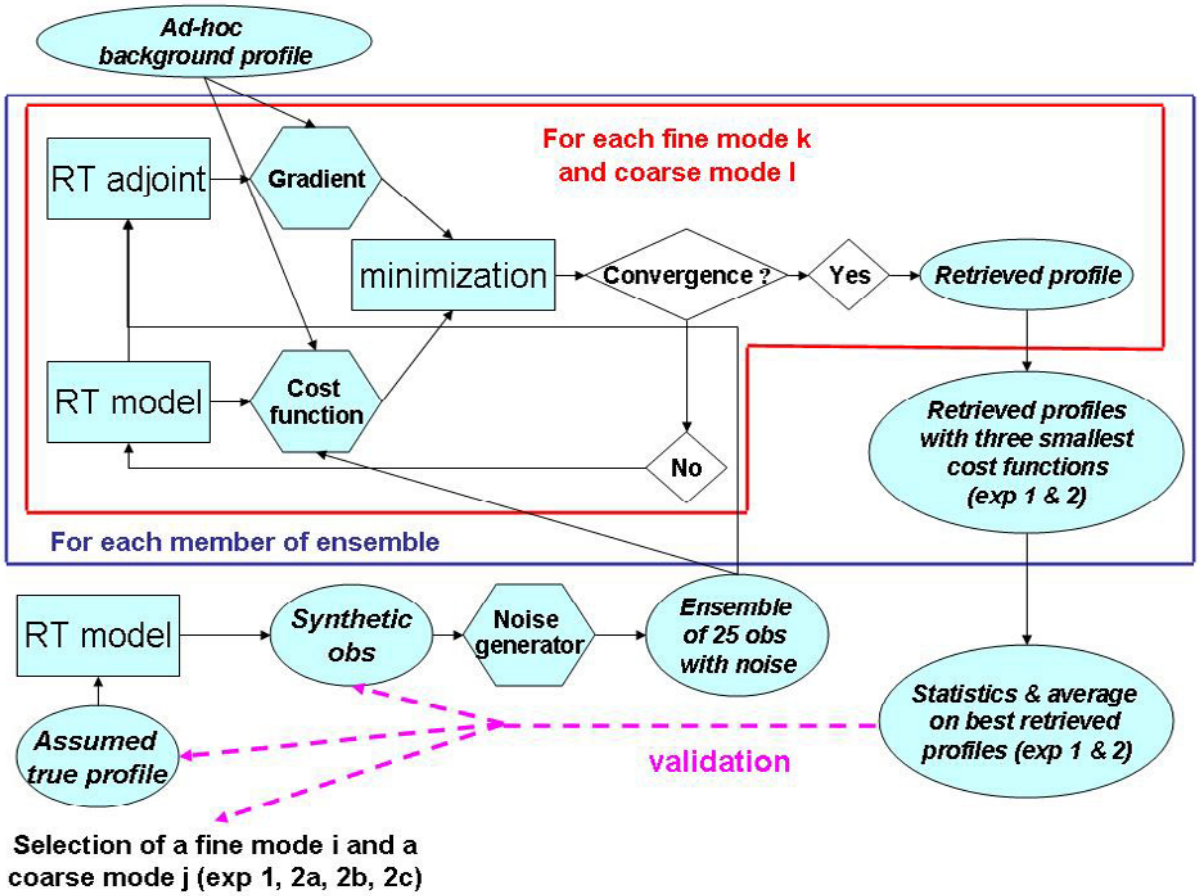

Figure 1. Schematic representation of retrieval scheme. Synthetic observations are generated from one pair of aerosol models of fine mode (i) and coarse mode (j). Noise is added randomly to these synthetic observations and a 25-member ensemble of synthetic observations is created. For each of these members, a retrieval is conducted for each possible pair of fine (k, $k = 1-4$) and coarse modes (l, $l = 1-5$). We retain the retrievals with the three smallest (exp 1) or the smallest (exp 2) cost functions.

where $\boldsymbol{H}$ is the observation operator, $\mathbf{R}$ is the error covariance matrix of the observation vector, and $\mathbf{B}$ is the error covariance matrix of the a priori x^{b}.

[9] At each iteration, computations of the cost function and its gradient are conducted and the model variable x can be iteratively computed as:

$$x^{n} = x^{n-1} + \alpha \nabla J\left(x^{n-1}\right) \tag{2}$$

where ∇J represents the gradient of the cost function, and α is the step length of each iteration. We use the adjoint method to compute efficiently the gradient of the cost function. To minimize the cost function, we use a quasi-Newton limited memory algorithm for bound constrained optimization called L-BFGS-B [*Byrd et al.*, 1994]. We only bounded the solution by defining a lower bound of zero for the entire vector x, defined below. The minimization stops as soon as at least one of the two stopping criteria stipulated in the minimization code is met. The first criterion requires the reduction of the cost function to be smaller than a threshold. The second criterion requires the module of the projection of the gradient to be smaller than a defined value. Since computing time is not an issue in our case, we can afford to demand high accuracy in the solution. We therefore set the first stopping criteria to a reduction in the cost function to be smaller than 10 times the precision of the machine. We demand as second stopping criteria the slope of the projected gradient to be smaller than 10^3 in every direction.

[10] If $\mathbf{H}$ is the linearized version of $\boldsymbol{H}$ and $\mathbf{H}^{\mathbf{T}}$ is the adjoint of the $\mathbf{H}$ operator, described in the next section, the gradient of the cost function can be written as:

$$\nabla J(x) = \mathbf{B}^{-1}\left(x - x^{\mathrm{b}}\right) + \mathbf{H}^{\mathrm{T}}\mathbf{R}^{-1}(H(x) - y^{o}) \tag{3}$$

2.2. Simplified Model and its Adjoint

[11] In this study, the direct model $\boldsymbol{H}$ corresponds to a simplified radiative transfer model that computes radiances at six wavelengths and simulates the lidar signal at two wavelengths. Two aerosol modes are considered in these computations, namely, the fine and coarse modes. Hereafter, variables corresponding to the accumulation mode will be indicated by an "f" as subscript whereas the coarse mode will be designated by a "c" as subscript. We consider a simplified atmosphere characterized by aerosol scattering

and absorption only. We consequently ignore gas absorption, Rayleigh scattering, and surface reflectance. We also neglect the effects of multiple scattering and assume single scattering both for the lidar and radiance calculations. With these simplifications, the lidar signal is simulated as:

$$\begin{aligned} \mathrm{LS}(z,\lambda) = C_{\mathrm{LS}} & \left[\beta_{\mathrm{f}}(\lambda)\omega_{\mathrm{f}}(\lambda)\sigma_{\mathrm{f}}(z,\lambda)\right. \\ & \left. + \beta_{\mathrm{c}}(\lambda)\omega_{\mathrm{c}}(\lambda)\sigma_{\mathrm{c}}(z,\lambda)\right] \\ & \cdot \exp\left(-2\int_z^{\mathrm{TOA}}\left[\sigma_{\mathrm{f}}(z',\lambda)+\sigma_{\mathrm{c}}(z',\lambda)\right]dz'\right) \end{aligned} \tag{4}$$

where $\omega(\lambda)$, $\beta(\lambda)$, and $\sigma(z, \lambda)$ are the wavelength-dependent single-scattering albedo, phase function at 180° (backscattering), and extinction coefficient (also height dependent, z), respectively. C_{LS} is a calibration constant set to one. The radiance is simulated as:

$$L(\lambda) = C_{\mathrm{L}}\left[\omega_{\mathrm{f}}(\lambda)\beta_{\mathrm{f},\Phi}(\lambda)\tau_{\mathrm{f}}(\lambda)+\omega_{\mathrm{c}}(\lambda)\beta_{\mathrm{c},\Phi}(\lambda)\tau_{\mathrm{c}}(\lambda)\right]/(4\pi\mu) \tag{5}$$

where $\beta_\Phi(\lambda)$ is the phase function at the considered scattering angle (120° here), μ is the cosine of the scattering angle, C_{L} is a constant set to one, and $\tau(\lambda)$ is the aerosol optical depth which relates to the aerosol extinction coefficient through:

$$\tau(\lambda) = \int_0^{\mathrm{TOA}} \sigma(z',\lambda)dz' \tag{6}$$

We define an atmosphere of 10 levels with the aerosols forming one cloud distributed in one or more atmospheric layers. We consider the radius of each aerosol mode (R_{gf} and R_{gc}) to be fixed throughout the atmospheric column. Equation 4 is discretized on the 10 vertical levels z_{i} as:

$$\begin{aligned} \mathrm{LS}(z_i,\lambda) = C_{\mathrm{LS}} & \left[\beta_{\mathrm{f}}(\lambda)\omega_{\mathrm{f}}(\lambda)\sigma_{\mathrm{f}}(z_i,\lambda)\right. \\ & \left. + \beta_{\mathrm{c}}(\lambda)\omega_{\mathrm{c}}(\lambda)\sigma_{c}(z_i,\lambda)\right] \\ & \cdot \exp\left(-2\sum_{j=i}^{\mathrm{TOA}}\left[\sigma_{\mathrm{f}}(z_j,\lambda)+\sigma_{\mathrm{c}}(z_j,\lambda)\right]\Delta z\right) \end{aligned} \tag{7}$$

where Δz is the layer thickness taken as 1 km throughout the atmosphere from the surface.

[12] Optical properties such as the phase function (β) and single-scattering albedo (ω) are prescribed and calculated offline using Mie theory. These calculations are conducted assuming a lognormal size distribution and using a prescribed modal radius (R_{g}), standard deviation (σ_0) and refractive index for each aerosol mode.

[13] Our observation vector y^{o} contains the synthetic lidar signal profiles at two wavelengths (0.53 and 1.06 μm) for our 10-layer atmosphere [equation (7)] and the synthetic radiances at six wavelengths, namely, 0.55, 0.66, 0.86, 1.23, 1.65, and 2.13 μm [equation (5)]. The observation vector y^{o} is therefore of dimension 26. The control vector x is composed of the extinction-coefficient profiles for the fine (σ_{f}) and coarse (σ_{c}) aerosol modes for the same 10 layers at a reference wavelength of 0.55 μm (i.e., x is of dimension 20). The extinction coefficient at other wavelengths can be deduced from the aerosol model and the extinction coefficient at 0.55 μm. The modal radii for each mode (R_{gf} and R_{gc}) are not retrieved directly and consequently not included in the control vector.

[14] This study represents an exploratory work on how to best exploit the synergy between MODIS radiances and CALIOP lidar backscattering profiles. While this model is highly simplified, it nevertheless fits the purpose of this study, which is to investigate how much information on the aerosol vertical profile and size distribution can be inferred from combined lidar and radiometric satellite observations. In light of these simplifications, the information content retrieved from these academic simulations should be seen as the maximum achievable from real observations.

[15] The adjoint model is derived using an automatic differentiation algorithm called TAPENADE [*Hascoët and Pascual*, 2004]. The advantage of the adjoint method is that it allows an exact calculation of the Jacobian and is numerically cheap, thus reducing the computational burden compared to other methods that would calculate numerically the gradient of the direct model from finite differences [*Le Dimet and Talagrand*, 1986]. In this study, however, computing time is not a limiting factor, and the use of the adjoint technique obeys more to the interest in studying the quality of the retrieval and its limitations, with a view to apply this method in three-dimensional models using a more complex and realistic radiative-transfer model.

2.3. Synthetic Observations

[16] In the present study, we test the retrieval scheme using synthetic observations. These are generated by running our simplified model defined above with given vertical profiles of the aerosol fine-mode and coarse-mode extinction coefficient, as well as prescribed size distribution and refractive index for each aerosol mode. The defined profile of extinction coefficient is taken within a realistic range. This information will be considered as the "true" state of the atmosphere to which the retrieval will be eventually compared.

[17] Aerosol properties are taken from the MODIS aerosol models presented by *Remer et al.* [2005]. These models consist of the refractive index, modal radius (R_{g}), and standard deviation (σ_0) for five coarse-mode and four fine-mode lognormal size distributions. These models are expected to be representative of the actual variability in aerosol size distribution and refractive index found in the real world. Each mode represents a typical aerosol type, from dry smoke to wet urban pollution, salt, and dust with refractive indices assigned accordingly [*Kaufman et al.*, 2003]. They are used in the MODIS lookup tables for aerosol retrieval over ocean. The properties of these fine and coarse modes are presented in Table 1. For simplicity, we do not consider any wavelength dependence for the refractive index. This assumption, even though it influences our results, should not induce any loss of generalities in our final conclusions as it is applied consistently for generating the synthetic observations and for running our retrievals.

[18] In order to reproduce the instrumental error, we have introduced noise into the synthetic observations. A Gaussian noise is added to synthetic observations to simulate the measurement error of each instrument. For the radiance, the standard deviation of the noise is taken as 2% of the true radiance at 0.55, 0.66, and 0.86 μm and 3% at 1.23, 1.65, and 2.13 μm. This error corresponds to the calibration uncertainties of the radiometer [*Miura et al.*, 2000]. The error in the lidar signal is a combination of the instrument

Table 1. Aerosol Models for the Aerosol Fine and Coarse Modes[a]

		Refractive Index	R_g	σ_0	R_{eff}	Comments
Fine Mode	1	1.45(1.40)–0.0035(0.0070)i	0.07	0.4	0.10	Small fine
	2	1.45(1.40)–0.0035(0.0070)i	0.06	0.6	0.15	Intermediate fine
	3	1.40(1.45)–0.0020(0.0035)i	0.08	0.6	0.20	Wet large fine
	4	1.40(1.45)–0.0020(0.0035)i	0.1	0.6	0.25	Wetter large fine
Coarse Mode	1	1.45(1.49)–0.0035(0.0035)i	0.4	0.6	0.94	Wet sea salt type
	2	1.45(1.49)–0.0035(0.0035)i	0.6	0.6	1.48	Wet sea salt type
	3	1.45(1.49)–0.0035(0.0035)i	0.8	0.6	1.98	Wet sea salt type
	4	1.53(1.49)–0.0010(0.0020)i	0.6	0.6	1.48	Dust-like type
	5	1.53(1.49)–0.0010(0.0020)i	0.5	0.8	2.50	Dust-like type

[a] R_g, σ_0, and R_{eff} are, respectively, the median radius (in μm), standard deviation of the lognormal size distribution, and the effective radius (μm). The perturbed values of refractive index for experiments 2 and 3 are given in parentheses. The aerosol models are from *Remer et al.* [2005].

noise and a calibration noise. The calibration noise applies uniformly over the vertical and is sometimes referred to as a bias but can be assumed to vary randomly from one retrieval to the next. Therefore in the context of one-dimensional-Var, it can be treated as a random error but with vertical correlation. The instrument noise is simulated with a standard deviation of the noise of 10% at 0.532 μm and 20% at 1.064 μm. This corresponds to the expected noise from CALIOP after averaging the signal to a resolution of 1 km in the vertical and 25 km in the horizontal (J. Pelon, personal communication, 2006). Calibration is performed in the 0.532-μm channel considering molecular scattering at high altitudes ($\sim$40 km) and is transferred to the 1.064-μm channel using a reflective target such as a high-level cloud, which introduces a strong correlation between the two calibration errors. Because of a poor understanding of the spectral correlation of the calibration error, we assume a standard deviation of the calibration noise for both wavelengths of 5% of the signal and a full correlation between the two lidar wavelengths (J. Pelon, personal communication, 2006).

[19] *Kaufman et al.* [2003] based their sensitivity tests to observational errors with errors of similar magnitude. They considered a random noise of 10 and 20% for the 0.532- and 1.064-μm lidar wavelengths, respectively, and calibration errors of 5 or 10%. While 5 and 10% calibration errors introduced 20 and 40% error in the optical thickness, they argued that the random noise in the observations did not systematically affect the retrieval. It should be noted though that in contrast to the variational method presented here their method would not treat the different sources of errors consistently. In contrast, we present in this paper a more systematic analysis of the impact of observational errors on the retrieval.

[20] For each experimental setup (described below), we consider an ensemble of 25 realizations of synthetic observations perturbed with noise. We only report the mean and standard deviation of the retrieved profiles for each of these ensembles. Sensitivity tests (not discussed here) with up to 150 realizations instead of 25 have shown that 25 members in the ensemble were sufficient.

2.4. Error Covariance Matrices

[21] The error covariance matrix for the observations, **R**, usually combines the instrumental and the model errors. However, since we use synthetic observations which are generated using the same model as used in the inversion, the only model errors would be of numerical nature, and these are expected to be negligible as compared to the instrumental errors. The diagonal terms for the lidar signal correspond to the combination of the instrument and calibration errors described in the previous section. The nondiagonal terms represent the vertical and spectral correlations in the calibration error of the lidar signal. The diagonal terms for the radiance terms correspond to 2% of the true radiance at the three wavelengths between 0.55 and 0.86 μm and 3% for the remaining three wavelengths. We assume the radiance-measurement errors to be uncorrelated with each other. We also assume the radiance and lidar-signal errors to be uncorrelated to each other. In summary, the **R** matrix can be expressed as

$$\mathbf{R} = \begin{pmatrix} R^{11}_{\mathrm{lid}} & & & R^{ii}_{\mathrm{lid}} & & 0 & \cdots & 0 \\ & \ddots & & & & \vdots & \vdots & \\ & & R^{ij}_{\mathrm{lid}} & & & R^{2020}_{\mathrm{lid}} & 0 & \cdots & 0 \\ 0 & & \cdots & & & 0 & R^{1}_{\mathrm{rad}} & 0 & 0 \\ \vdots & & & & & \vdots & 0 & \ddots & 0 \\ 0 & & \cdots & & & 0 & 0 & \cdots & R^{6}_{\mathrm{rad}} \end{pmatrix} \quad (8)$$

where $R^{ij}_{\mathrm{lid}} = (\delta^{ij}\, n\lambda^2 + c\lambda^2)\, \mathrm{LS}^i\, \mathrm{LS}^j$; both superindex i and j span the vertical and spectral ranges for the lidar signal, δ^{ij} is 1 if $i = j$ and 0 otherwise, n_λ and c_λ are the percentage magnitude of the random and calibration errors, respectively, as previously defined in section 2.3.

[22] Since we have limited and unreliable knowledge on the a priori information, we neglect the a priori term from the cost function [equation (1)] and define it solely as the observation term. Therefore there is no need to define an error covariance matrix for the background.

Table 2. Percentage of Successful Retrievals for Each Possible Combination of Fine and Coarse Modes Used to Generate the Observations in Experiment 1[a]

			$\tau_f > \tau_c$ Coarse Mode					$\tau_f < \tau_c$ Coarse Mode				
		Minima	1	2	3	4	5	1	2	3	4	5
Fine Mode	1	Min 1	92	64	**96**	80	72	**72**	48	88	60	64
		Min 2	4	36	4	20	24	20	4	4	20	20
		Min 3	4	0	0	0	4	0	8	0	8	4
	2	Min 1	64	64	88	72	64	28	36	40	44	28
		Min 2	20	28	8	20	32	20	16	12	16	28
		Min 3	16	0	4	4	0	40	44	48	36	44
	3	Min 1	44	20	28	36	36	24	24	4	16	0
		Min 2	32	16	28	20	12	48	48	76	40	64
		Min 3	4	32	16	12	8	16	12	12	20	24
	4	Min 1	44	48	52	40	20	64	60	68	60	60
		Min 2	40	28	24	16	36	4	16	16	28	8
		Min 3	16	12	20	20	28	24	12	16	8	4

[a] Solutions with the three smallest residual cost functions are shown. As an example, when the fine mode dominates in optical depth and the synthetic observations are constructed using fine mode 1 and coarse mode 1, this particular combination is retrieved 92% of the times with the smallest cost function, 4% of the times with the second smallest cost function, and 4% of the times with the third smallest cost function. Numbers in bold correspond to cases presented in Figures 2 and 3.

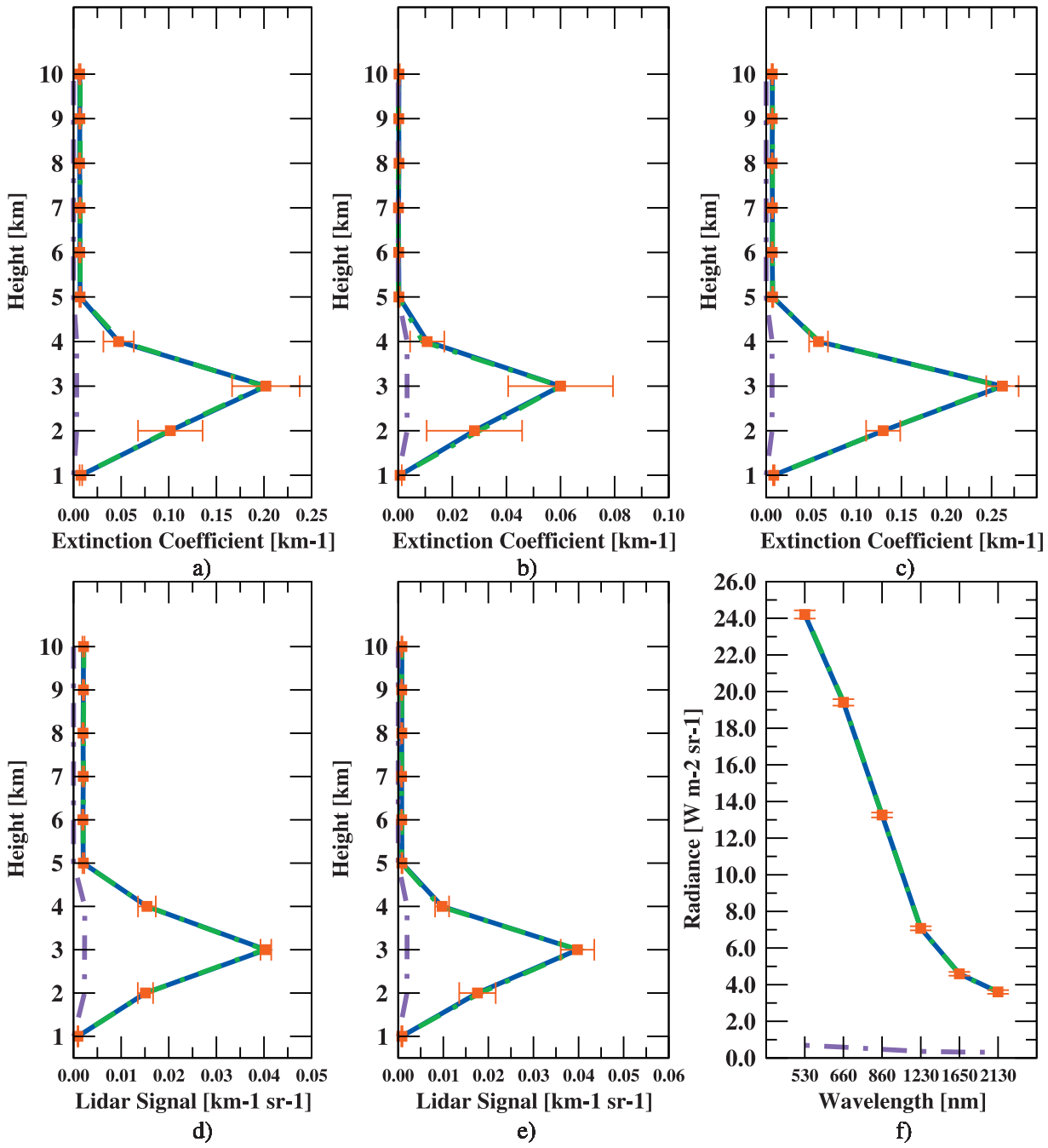

Figure 2. Profiles of the aerosol extinction coefficient for (a) the fine mode, (b) the coarse mode, and (c) total extinction coefficient. Profiles of the lidar signal at (d) 0.532 μm and (e) 1.064 μm and (f) spectral radiances. Each panel shows the first guess (black dashed/purple), the values treated as truth (gray/green), and the retrievals (black continuous/blue). The plots are for exp 1, with synthetic observation generated with fine mode 1 and coarse mode 3 and the aerosol load of the fine mode larger than that of the coarse mode. The error bars for the retrievals show the standard deviation around the mean for the 25 member retrievals. See color version of this figures in the HTML.

2.5. Retrieval Scheme

[23] We initialize the retrieval from a first-guess profile of the extinction coefficient at 0.55 μm. Tests have shown that there is no sensitivity of the results to the choice of the first guess. The cost function and the corresponding gradient are evaluated according to equations (1) and (3) described above. We do not attempt to retrieve the aerosol model directly in the variational retrieval. Consequently, the control vector does not include aerosol size and refractive index. However, we follow *Kaufman et al.* [2003] and indirectly retrieve the aerosol model from the preselected set of aerosol models shown in Table 1. We do so by splitting the retrieval in two successive steps. First, we run the retrieval, for each member of the ensemble of noise-perturbed synthetic observations, for each of the 20 possible

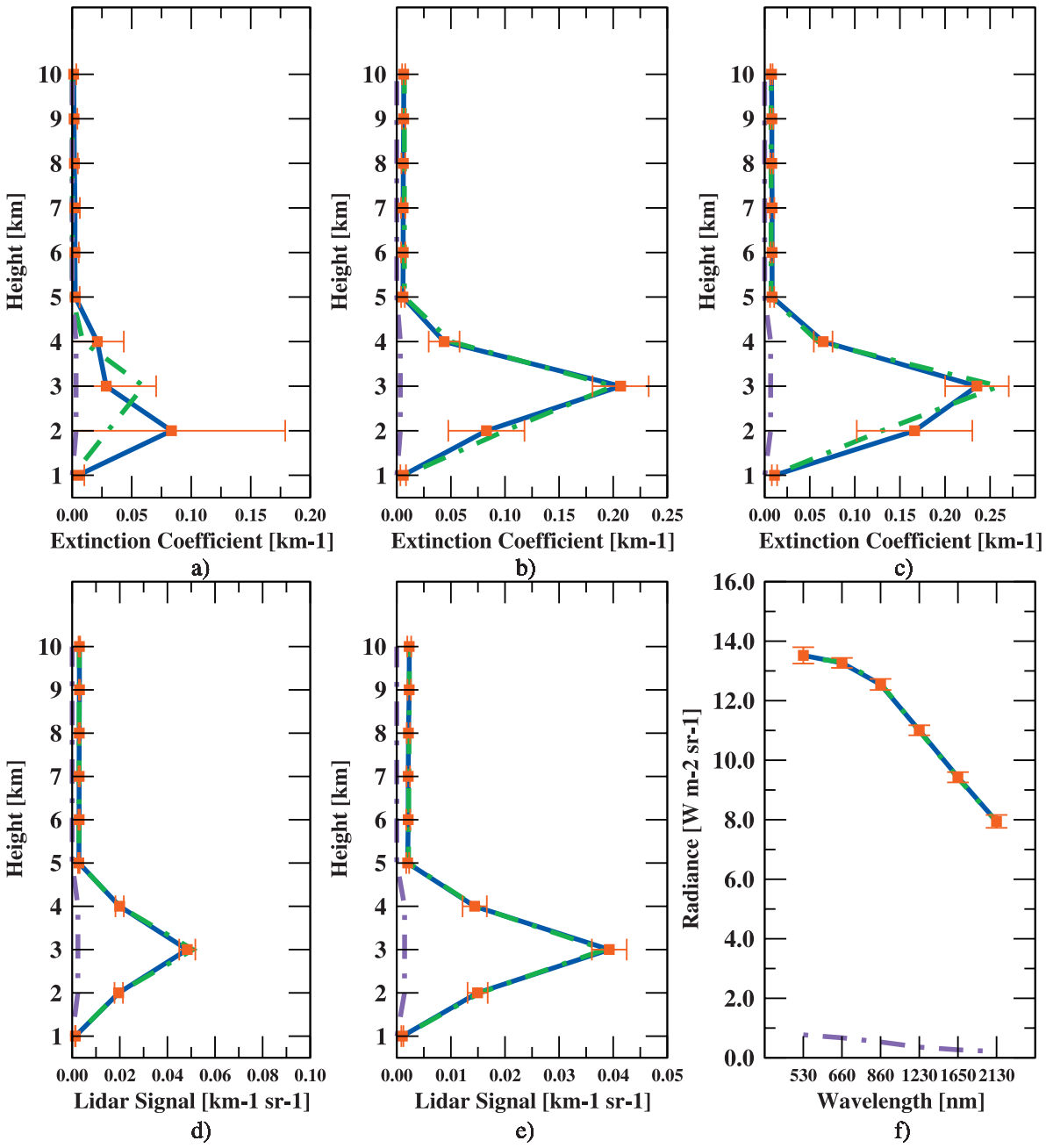

Figure 3. Same as Figure 2 but for experiment 1 with synthetic observations generated using fine mode 1 and coarse mode 1 and the fine mode aerosol load smaller than that of the coarse mode. See color version of this figures in the HTML.

Table 3. Percentage of Successful Retrievals of the Coarse Mode Aerosol Model When Only the Fine Mode is Perturbed (Experiment 2a)[a]

		$\tau_f > \tau_c$ Coarse Mode					$\tau_f < \tau_c$ Coarse Mode				
		1	2	3	4	5	1	2	3	4	5
Fine Mode	1	0	0	72	0	100	8	100	100	96	80
	2	0	0	100	0	0	100	100	4	60	0
	3	0	0	100	0	0	100	100	4	60	0
	4	0	0	100	0	0	100	96	0	60	0

[a]Only retrievals with the smallest cost function are considered.

Table 4. Retrieved Fine Mode Refractive Index (Real Part) for Experiment 2a Averaged From the 25 Members of the Ensemble of Synthetic Observations Constructed From Each Combination of Fine and Coarse Modes[a]

Perturbed Refractive Index			$\tau_f > \tau_c$ Coarse Mode					$\tau_f < \tau_c$ Coarse Mode				
			1	2	3	4	5	1	2	3	4	5
Fine Mode	1	**1.40**	1.45	1.45	1.45	1.45	1.45	1.45	1.43	1.40	1.40	1.41
	2	**1.40**	1.45	1.45	1.45	1.45	1.45	1.43	1.40	1.40	1.42	1.41
	3	**1.45**	1.45	1.45	1.45	1.45	1.45	1.43	1.40	1.40	1.42	1.41
	4	**1.45**	1.45	1.45	1.45	1.45	1.45	1.43	1.40	1.40	1.42	1.41

[a]Underlined numbers correspond to cases where the true refractive index was retrieved within ±0.01 of the perturbed value.

Table 5. Retrieved Fine Mode Modal Radius (μm) for Experiment 2a Averaged From the 25 Members of the Ensemble of Synthetic Observations Constructed From Each Combination of Fine and Coarse Modes[a]

			$\tau_f > \tau_c$ Coarse Mode					$\tau_f < \tau_c$ Coarse Mode				
		Radius	1	2	3	4	5	1	2	3	4	5
Fine Mode	1	**0.070**	0.070	0.070	0.070	0.070	0.070	0.072	0.084	0.1	0.099	0.095
	2	**0.06**	0.070	0.070	0.070	0.070	0.070	0.08	0.1	0.1	0.088	0.093
	3	**0.08**	0.070	0.070	0.070	0.070	0.070	0.084	0.1	0.099	0.088	0.093
	4	**0.1**	0.070	0.071	0.070	0.070	0.070	0.081	0.1	0.1	0.086	0.092

[a]Underlined numbers correspond to cases where the modal radius was retrieved within ±0.005 μm.

combinations out of the four fine and five coarse-mode aerosol models. Then, we retrieve the combination of aerosol models and extinction-coefficient profiles by retaining only those with the smallest residual cost function. By limiting the solution of the aerosol models to the predefined models, we decrease the dimension of the aerosol model space and thus avoid complications associated with the inclusion of explicit Mie calculations into the adjoint model.

[24] We conducted three sets of experiments. In the first one (exp 1), we took the aerosol properties as presented in Table 1, while in the second (exp 2) and third (exp 3) ones, we perturbed the real and imaginary part of the refractive index, respectively, when generating the observations. We conducted these last two experiments in three different ways, first perturbing only the fine-mode refractive index (exps 2a and 3a), then only the coarse-mode refractive index (exps 2b and 3b), and finally perturbing the refractive indices from both modes (exps 2c and 3c) (Table 1). The rationale of these experiments with microphysical perturbation was to investigate how the retrieval would behave if the observations were built from an aerosol model which does not belong to the set of aerosol models used for the retrievals.

[25] We can now summarize the experimental setup. In each experiment, we considered in turn each possible pair of unmodified (exp 1) or modified (exps 2 and 3) fine and coarse modes and two different splits of an aerosol optical depth of 0.5 between the two aerosol modes (either the fine mode or the coarse mode is taken as dominant with a 4:1 ratio in optical thickness). For each of these 40 cases, an ensemble of 25 synthetic observations was generated using random noise, as described above. For each resulting set of observations, we conducted the retrieval for each one of the 20 possible pairs of fine and coarse aerosol models. We retain the combination with the smallest residual cost function.

[26] We present average results for the ensemble of 25 synthetic observations with noise. The final products of the minimization therefore consist of the average retrieved extinction-coefficient profiles and the average aerosol optical properties. In order to evaluate the quality of the retrieval, we compare (1) the retrieved extinction-coefficient profiles with the ''true'' state of the atmosphere, (2) the simulated observations using the retrieved profiles with the synthetic observations, and (3) the average retrieved aerosol properties (size and refractive index) with those of the ''true'' aerosol models.

3. Results

3.1. Experiment 1

[27] The results for exp 1 are summarized in Table 2, and two cases (out of 40) are illustrated in Figures 2 and 3. We consider the true combination to be retrieved when the percentage of successful retrieval in the first minimum for each ensemble is larger than or equal to 50%. For the case of an aerosol load with fine mode predominating over the coarse mode, the true combination is retrieved whenever the observations are generated with fine modes 1 and 2 and for observations generated with fine mode 4 and coarse mode 3. For the case of coarse-mode aerosols predominating over fine-mode aerosols, the true combination is found whenever the observations are generated with fine modes 1 and 4. It is noteworthy that most of the time, the true combination is found among the best three solutions. For both aerosol loads analyzed, a large fraction of the time, the unsuccessful retrievals are explained by a failure in retrieving the correct fine-mode model.

[28] Under a predominance of fine aerosol, successful retrieval of the aerosol models also implies the retrieval of the true profiles of extinction coefficient (Figure 2). However, the conclusion does not necessarily hold when $\tau_f < \tau_c$ (see Figure 3). For all successful retrievals except for observations generated with fine mode 1 and coarse mode 3, the average vertical profile of the extinction coefficient for the fine mode does not reproduce on average the exact shape of the true profile. This is in spite of the retrieval of the true combination of aerosol models. Still, the vertical distribution of the total extinction coefficient corresponding to the retrieved profiles follows very closely the true vertical distribution (Figure 3c). This means that under real conditions and a predominant coarse mode, we would have more confidence in retrieving the total aerosol extinction coefficient than that of the fine mode. For observations generated with fine mode 1 and coarse mode 3 and a predominance of coarse aerosols, the scheme retrieves the true profiles. Whether the fine or coarse mode predominates, the quality of the retrieval for most of the cases is independent of the success of finding the true combination.

[29] Even though there is a good agreement between the observations and the model output in both cases analyzed

Table 6. Percentage of Successful Retrieval of the Fine Mode Aerosol Model When Only the Coarse Mode is Perturbed (Experiment 2b)[a]

		$\tau_f > \tau_c$ Coarse Mode					$\tau_f < \tau_c$ Coarse Mode				
		1	2	3	4	5	1	2	3	4	5
Fine Mode	1	100	100	100	100	100	100	96	0	92	52
	2	0	0	0	0	0	0	16	0	4	4
	3	0	0	0	0	0	0	24	24	0	0
	4	8	8	0	4	0	0	84	80	4	4

[a]Only retrievals with the smallest cost function are considered.

Table 7. Retrieved Coarse Mode Refractive Index (Real Part) for Experiment 2b Averaged From the 25 Members of the Ensemble of Synthetic Observations Constructed From Each Combination of Fine and Coarse Modes[a]

Perturbed Refractive Index		$\tau_f > \tau_c$ Coarse Mode					$\tau_f < \tau_c$ Coarse Mode				
		1	2	3	4	5	1	2	3	4	5
		1.49					**1.49**				
Fine Mode	1	1.50	1.50	1.47	1.53	1.53	1.45	1.45	1.45	1.53	1.53
	2	1.45	1.45	1.45	1.46	1.46	1.45	1.45	1.45	1.50	1.51
	3	1.45	1.45	1.45	1.45	1.45	1.45	1.45	1.45	1.50	1.51
	4	1.45	1.45	1.45	1.45	1.45	1.45	1.45	1.45	1.50	1.51

[a]Underlined numbers correspond to cases where the true refractive index was retrieved within ±0.02 of the perturbed value.

Table 9. Retrieved Fine Mode Refractive Index (Real Part) for Experiment 2c Averaged From the 25 Members of the Ensemble of Synthetic Observations Constructed From Each Combination of Fine and Coarse Modes[a]

Perturbed Refractive Index		$\tau_f > \tau_c$ Coarse Mode					$\tau_f < \tau_c$ Coarse Mode				
		1	2	3	4	5	1	2	3	4	5
Fine Mode	1 **1.40**	1.45	1.45	1.45	1.45	1.45	1.45	1.45	1.43	1.45	1.44
	2 **1.40**	1.45	1.45	1.45	1.45	1.45	1.45	1.42	1.40	1.45	1.45
	3 **1.45**	1.45	1.45	1.45	1.45	**1.45**	1.45	1.42	1.40	1.45	**1.45**
	4 **1.45**	1.45	1.45	1.45	1.45	1.45	1.45	1.41	1.40	1.44	1.45

[a]Numbers in bold correspond to cases presented in Figures 4 and 5. Underlined numbers correspond to cases where the true refractive index was retrieved within ±0.01 of the perturbed value.

with a small standard deviation (Figures 2d–2f and 3d–3f), a large standard deviation is observed in the vertical profile of the extinction coefficient (Figures 2a, 2b, 3a, and 3b). The large sensitivity to the introduced noise is due to the fact that several vertical distributions of the fine mode can provide the same match to the lidar observations. This appears to be caused by compensating effects between the backscatter and attenuation terms because of the fine mode in the lidar equation. The large standard deviation shown in Figure 3a reflects the fact that certain solutions of the ensemble attribute some of the coarse-mode extinction coefficient to the fine mode. Finally, a smaller standard deviation than the fine and coarse modes is observed for the total extinction coefficient in both cases (Figures 2f and 3f). This reflects that the scheme retrieves better individually the total extinction coefficient than those of the fine and coarse modes.

[30] Similar results are obtained when considering either the fine-mode aerosol layer above the coarse-mode aerosol layer or the opposite case (figures not shown). When repeating exp 1 only with instrumental noise, the results do not differ with the ones just presented (tables and figures not shown). This reflects the ability of the retrieval scheme to compensate for calibration error.

3.2. Experiment 2

[31] The results of exp 2 are presented in Tables 3 to 12, while Figures 4 and 5 illustrate two cases from exp 2c. We examine the retrieved nonperturbed aerosol model (exps 2a and 2b) and the averaged retrieved value of the real part of the refractive index and radius of the perturbed aerosol model (exps 2a, 2b, and 2c). These values are constructed as the average of the best solution from each of the 25 members of the ensemble of synthetic observations.

[32] When only the real part of the fine-mode refractive index is perturbed (exp 2a), the correct coarse mode is retrieved most of the time if it predominates over the fine mode, whereas in the opposite case, the "true" coarse mode is only found in some cases (Table 3). Because the actual fine-mode aerosol model used to produce the synthetic observations is not in the set of aerosol models used for the retrieval, we cannot expect the scheme to "retrieve" simultaneously the fine-mode refractive index and modal radius. We can see from Tables 4 and 5 that most of the time either one of these two parameters can be retrieved exactly or to a reasonable accuracy. There are, however, cases (e.g., fine mode 2 for $\tau_f > \tau_c$) where neither the refractive index nor the modal radius of the fine mode are retrieved. The frequency of successful retrievals of the true coarse mode keeps no relation with the average "retrieved" refractive index and mode radius of the fine mode.

[33] When only the real part of the coarse-mode refractive index is perturbed (exp 2b), the percentage of successful retrieval decreases for $\tau_f < \tau_c$ with respect to exp 2a in terms of finding the true unperturbed fine mode as the first minimum (Table 6). The real fine mode is retrieved all the time only for fine mode 1 and any given coarse mode when $\tau_f > \tau_c$. When $\tau_f < \tau_c$, the true fine mode is found only for isolated cases. The exact perturbed refractive index is never retrieved, but several cases present solutions fairly close to the perturbed value. Even though the true coarse mode is

Table 8. Retrieved Coarse Mode Modal Radius (μm) for Experiment 2b Averaged From the 25 Members of the Ensemble of Synthetic Observations Constructed From Each Combination of Fine and Coarse Modes[a]

		$\tau_f > \tau_c$ Coarse Mode					$\tau_f < \tau_c$ Coarse Mode				
		1	2	3	4	5	1	2	3	4	5
Radius		**0.4**	**0.6**	**0.8**	**0.6**	**0.5**	**0.4**	**0.6**	**0.8**	**0.6**	**0.5**
Fine Mode	1	0.63	0.63	0.72	0.51	0.5	0.58	0.6	0.8	0.6	0.53
	2	0.8	0.8	0.8	0.8	0.8	0.4	0.6	0.61	0.6	0.6
	3	0.8	0.8	0.8	0.8	0.8	0.4	0.6	0.61	0.6	0.6
	4	0.8	0.8	0.8	0.8	0.8	0.4	0.59	0.6	0.6	0.6

[a]Underlined numbers correspond to cases where the modal radius was retrieved within ±0.05 μm.

Table 10. Retrieved Coarse Mode Refractive Index (Real Part) for Experiment 2c Averaged From the 25 Members of the Ensemble of Synthetic Observations Constructed From Each Combination of Fine and Coarse Modes[a]

Perturbed Refractive Index		$\tau_f > \tau_c$ Coarse Mode					$\tau_f < \tau_c$ Coarse Mode				
		1	2	3	4	5	1	2	3	4	5
		1.49					**1.49**				
Fine Mode	1	1.52	1.52	1.52	1.52	1.53	1.45	1.45	1.45	1.45	1.46
	2	1.45	1.45	1.45	1.45	1.45	1.45	1.45	1.45	1.45	1.45
	3	1.45	1.45	1.45	1.45	**1.45**	1.45	1.45	1.45	1.45	**1.45**
	4	1.45	1.45	1.45	1.45	1.45	1.45	1.45	1.45	1.45	1.45

[a]Numbers in bold correspond to cases presented in Figures 4 and 5. Underlined numbers correspond to cases where the true refractive index was retrieved within ±0.02 of the perturbed value.

Table 11. Retrieved Fine Mode Modal Radius (μm) for Experiment 2c Averaged From the 25 Members of the Ensemble of Synthetic Observations Constructed From Each Combination of Fine and Coarse Modes[a]

			$\tau_f > \tau_c$ Coarse Mode					$\tau_f < \tau_c$ Coarse Mode				
	Radius		1	2	3	4	5	1	2	3	4	5
Fine Mode	1	**0.07**	0.07	0.07	0.07	0.07	0.07	0.07	0.07	0.07	0.07	0.07
	2	**0.06**	0.07	0.07	0.07	0.07	0.07	0.07	0.081	0.098	0.070	0.071
	3	**0.08**	0.07	0.07	0.07	0.07	**0.07**	0.07	0.082	0.094	0.07	**0.068**
	4	**0.1**	0.07	0.07	0.07	0.07	0.07	0.07	0.088	0.095	0.072	0.068

[a]Numbers in bold correspond to cases presented in Figures 4 and 5. Underlined numbers correspond to cases where the modal radius was retrieved within ±0.005 μm.

not within the predefined aerosol models, it is noteworthy that for a few observation cases such as those created using coarse mode 4 and fine modes 2 to 4, the scheme is able to retrieve approximately the perturbed refractive index and the modal radius simultaneously (Tables 7 and 8).

[34] Finally, in exp 2c, the true state of the atmosphere is defined by a combination of two aerosol models, none of which forms part of the set of aerosol models used for the retrieval. The way we examine the performance of the retrieval is through the average aerosol properties, as done previously, and the comparison of the retrieved and inversed profiles with the truth. Compared to the results of exp 2a, the scheme shows an improvement in the retrieval of the fine-mode radius (see Tables 5 and 11) and a slightly better retrieval of the fine-mode refractive index (Tables 4 and 9). Both improvements occur when $\tau_f < \tau_c$, while for the case of $\tau_f > \tau_c$, no change is observed between exps 2a and 2c. On the other hand, a decrease in the number of successful retrievals of refractive index (Tables 7 and 10) of the coarse mode is observed. Again, this is stronger when $\tau_f < \tau_c$. The scheme is able to retrieve simultaneously the modal radii of both aerosol modes for observations generated with fine mode 1 and coarse mode 5 when $\tau_f > \tau_c$ and fine mode 1, coarse modes 2 to 4, and fine mode 3, coarse mode 2 when $\tau_f < \tau_c$ (see Tables 11 and 12). However, for none of the possible set of generated observations, the retrieval scheme is able to find the refractive index of the coarse mode, neither when $\tau_f > \tau_c$ nor when $\tau_f < \tau_c$. Furthermore, the scheme is unable to simultaneously retrieve the refractive index and modal radii of both modes. Figure 4 presents the retrieved profiles of extinction coefficient for the fine (Figure 4a) and coarse modes (Figure 4b) and total extinction coefficient (Figure 4c) for the case of a predominance of fine-mode aerosols. The lidar signal at 0.532 and 1.064 μm (Figures 4d and 4e, respectively) and spectral radiances (Figure 4f) corresponding to the retrieved profiles are also presented. The retrieved profiles of both modes capture the main features of the true vertical distribution. While the fine mode underestimates the true extinction coefficient, the coarse mode overestimates the true profile most of the time. Yet the retrieved true profile remains within the variability of the true retrieved coarse mode. Furthermore, the profile of total extinction coefficient is also underestimated, because of the underestimation in the fine mode. The difficulty in retrieving the correct vertical profile is explained by the error in simulating the spectral dependence of the radiance. In most of the cases, the lidar signal at both wavelengths is well simulated; however, the lidar signal at 0.532 μm corresponding to the retrieved profiles simulates slightly better the true profile than the one at 1.064 μm. In the rest of the cases, the main differences with the true profile are observed at 1.064 μm, which shows a higher tendency to overestimate the true lidar signal. The opposite case of $\tau_f < \tau_c$ presents more difficulties in retrieving the true profile of extinction coefficient for the fine mode but improves the retrieval of the coarse mode (Figures 5a and 5b). It underestimates the fine mode and overestimates the coarse mode but shows an improvement in the retrieval of the total extinction-coefficient profile (Figure 5c). Errors in the retrieval are due to the misfit in simulating the true lidar signal at both wavelengths (Figures 5d and 5e) and the spectral dependance of the radiance (Figure 5f). The misfit to the spectral radiance is significantly larger than the measurement error, thus suggesting some inconsistency in our one-dimensional-Var system. This is not surprising of course because of the large perturbation in the aerosol mycrophysical properties. There is therefore some prospect of improvement by increasing the size of the predefined set of aerosol models.

3.3. Experiment 3

[35] In contrast to exp 2, when the imaginary part of the refractive index is perturbed, a higher success rate in the retrieval of the unperturbed aerosol mode is observed in exps 3a and 3b. In exp 3a, the true coarse mode is retrieved most of the time when $\tau_f > \tau_c$ and always when $\tau_f < \tau_c$. In exp 3b, the scheme has a higher success rate (as compared with exp 3a) in the retrieval of the correct fine mode when $\tau_f > \tau_c$ but a lower success rate when $\tau_f < \tau_c$. A higher retrieval rate of the modal radius is also observed in both experiments. With respect to exp 3c, the same conclusion as in exp 2c is valid, with the

Table 12. Retrieved Coarse Mode Modal Radius (μm) for Experiment 2c Averaged From the 25 Members of the Ensemble of Synthetic Observations Constructed From Each Combination of Fine and Coarse Modes[a]

		$\tau_f > \tau_c$ Coarse Mode					$\tau_f < \tau_c$ Coarse Mode				
	1	2	3	4	5	1	2	3	4	5
Radius	**0.4**	**0.6**	**0.8**	**0.6**	**0.5**	**0.4**	**0.6**	**0.8**	**0.6**	**0.5**
Fine Mode 1	0.55	0.52	0.54	0.52	0.5	0.6	0.6	0.8	0.6	0.75
Fine Mode 2	0.8	0.8	0.8	0.8	0.8	0.42	0.6	0.74	0.6	0.62
Fine Mode 3	0.8	0.8	0.8	0.8	**0.8**	0.41	0.6	0.74	0.6	**0.62**
Fine Mode 4	0.8	0.8	0.8	0.8	0.8	0.4	0.6	0.73	0.6	0.62

[a]Numbers in bold correspond to cases presented in Figures 4 and 5. Underlined numbers correspond to cases where the modal radius was retrieved within ±0.05 μm.

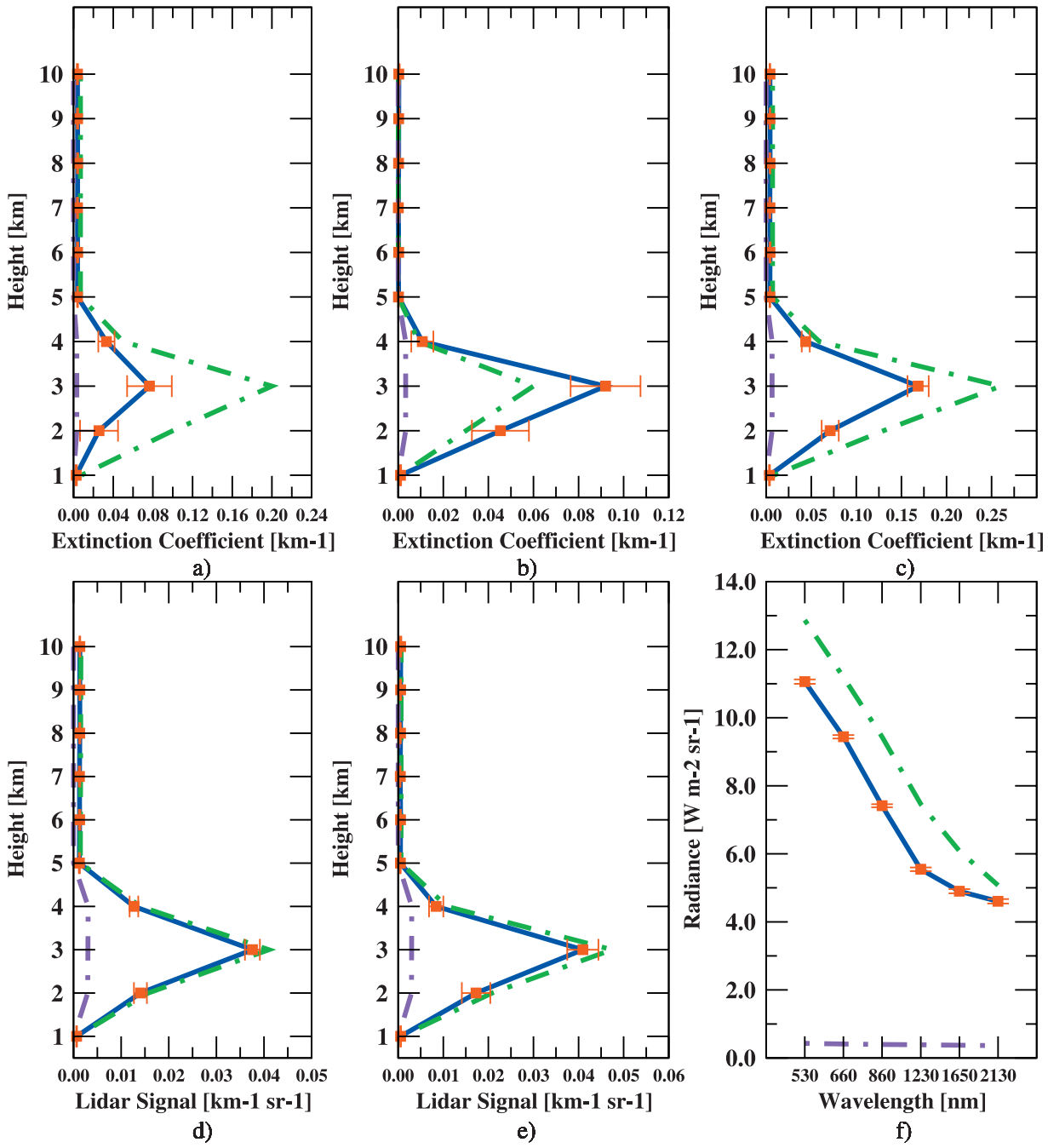

Figure 4. Same as Figure 2 but for exp 2c, i.e., perturbation of refractive index of the fine and coarse modes and synthetic observation generated with fine mode 3 and coarse mode 5. See color version of this figures in the HTML.

only difference being the higher retrieval rate as compared to exp 2c (tables and figures not shown).

4. Conclusions

[36] An exploratory study on variational retrieval was conducted in order to investigate how to best exploit the synergy between MODIS radiances and CALIPSO lidar-attenuated backscattering profiles. A joint retrieval should combine information on the vertical distribution of aerosols from the lidar and information on size from the radiometer. The retrieval scheme was applied to a simplified radiative transfer model to retrieve the extinction-coefficient profile of fine and coarse aerosol modes. Synthetic observations were constructed from an aerosol model and vertical profile, taken as the truth, in order to mimic the lidar and radiometric measurements. Noise was introduced into the synthetic observations in order to reproduce the instrumental and calibration errors. Experiments were conducted for a constant aerosol load but varying from a predominant fine mode to a predominant coarse mode. Different degrees of perturbation to the real part of the refractive index were also introduced in some of the experiments. For the ideal case

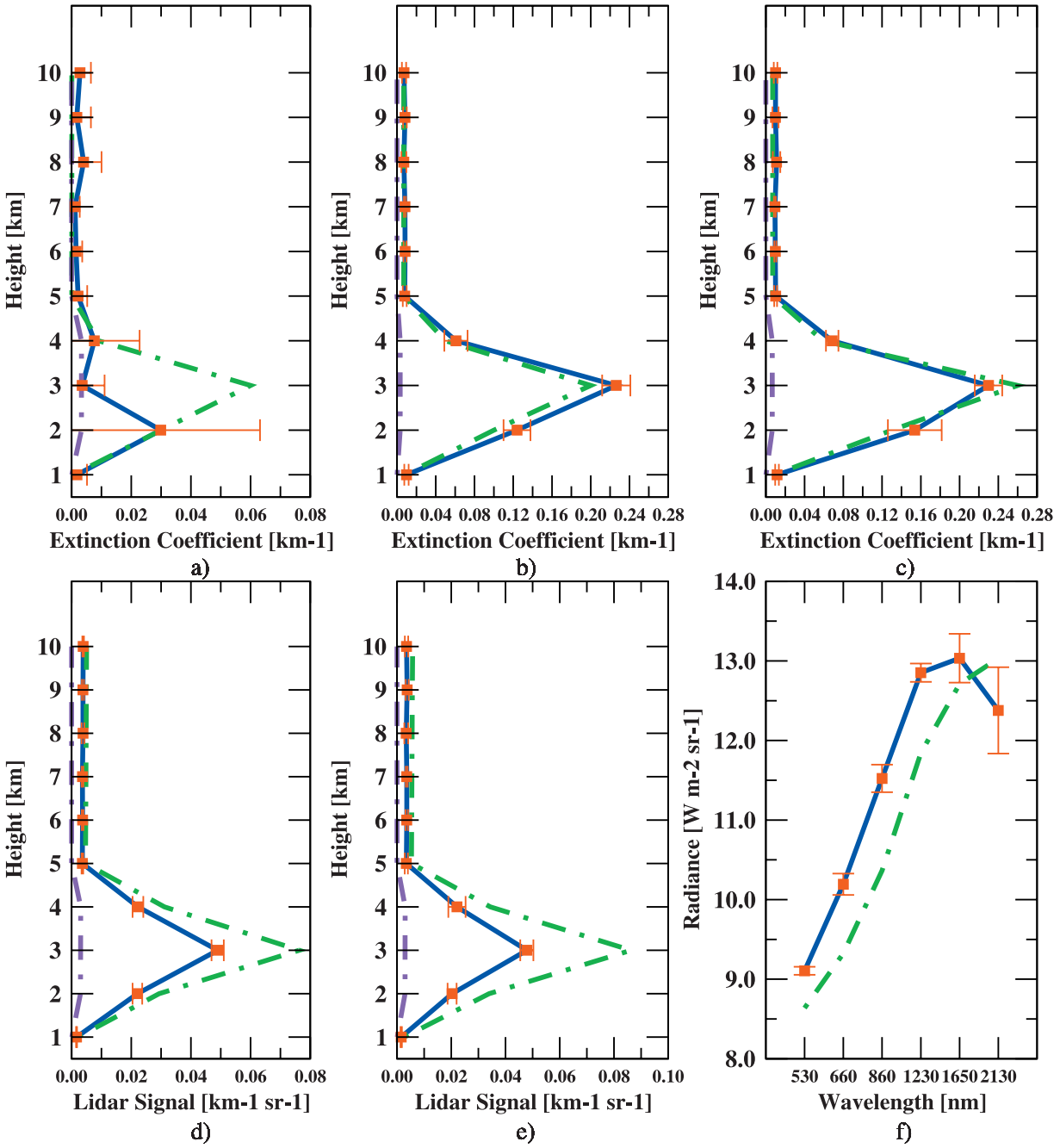

Figure 5. Same as Figure 4 but for the case of the aerosol load of the coarse mode larger than that of the fine mode. See color version of this figures in the HTML.

when the true aerosol model belongs to our set of predefined aerosol models used in the retrieval, the scheme shows an equivalent success rate in retrieving the true aerosol combination for both cases of aerosol loads analyzed. For the case of fine mode predominating over the coarse mode, the true profile is successfully retrieved for both modes and for the total extinction coefficient. For the opposite case of predominant coarse aerosol model, the scheme manages to retrieve the true profile of extinction coefficient of the coarse mode but is not able to retrieve exactly the true profile of the fine mode even when the correct aerosol models are found. It nevertheless retrieves accurately the profile of the total extinction coefficient. Interestingly, the success of the retrieval for most of the cases is independent of finding the true combination. This reflects the fact that retrieving the correct profile does not represent an indicator of success in the retrieval of the true aerosol combination. The standard deviation of the total extinction coefficient is smaller than those of the fine and coarse modes. This implies that the scheme retrieves better individually the total extinction coefficient than the fine and coarse ones but shows the same performance for the ensemble. Equivalent results are observed when exp 1 is repeated without calibration noise, revealing the ability of the scheme to compensate for errors in the calibration. Similar conclusion can

be drawn with a vertical distribution of aerosols with the fine-mode layer above the coarse-mode layer and vice versa.

[37] For the more challenging case when the true aerosol model does not belong to our set of predefined aerosol models used in the retrieval, the scheme has difficulties in retrieving the true profile for fine and coarse modes. It underestimates the extinction coefficient of the fine mode and overestimates that of the coarse mode. However, when the coarse mode predominates over the fine mode, the scheme shows an improvement in the retrieval of the total extinction coefficient. The errors in the retrieval when $\tau_f > \tau_c$ are mainly due to the misfit in reproducing the spectral dependence of the radiance, whereas when $\tau_f < \tau_c$, the differences between retrieved and true profile are also due to the misfit in the lidar signal at both wavelengths. The scheme is able to obtain the modal radii of both modes simultaneously, but it is not able to obtain simultaneously the perturbed aerosol refractive indices and the true mode radii for both modes. All in all, the scheme shows a better retrieval of aerosol properties, both refractive index and modal radii, for a predominance of coarse-mode aerosols.

[38] When perturbing the imaginary part of the refractive index, similar results to exp 2 are found. The main difference between these experiments is an increase in the retrieval rate when compared to results obtained by perturbing the real part of the refractive index.

[39] The MODIS wavelengths are more sensitive to the coarse mode than to the fine mode [*Kaufman et al.*, 2003]. This may explain the general improvement in the retrieval when both modes are perturbed and $\tau_f < \tau_c$ and the successful retrieval of the fine-mode extinction-coefficient profile when $\tau_f > \tau_c$.

[40] The results and conclusions of exp 2 rely strongly on the definition of the aerosol models. These models serve the purpose of reducing the solution space and avoid including explicit Mie calculations in the retrieval scheme. We would like to highlight the fact that in many cases with perturbed microphysics, the residual error in the fit between the observed and simulated radiance and lidar signal is larger than the observational error. This means that synthetic observations have not been exploited to their full potential, and there is therefore prospect for achieving better retrievals by including more aerosol models in our predefined set.

[41] While this model is highly simplified, it nevertheless fits the purpose of this study, which is to investigate how much information on the aerosol vertical profile and size distribution can be inferred from combined lidar and radiometric satellite observations. In light of these simplifications, the retrieved information content from these academic simulations should be seen as the maximum achievable for the current set of predefined aerosol models. This simplified model can also be used to test enhanced synergies between instruments or the improvement that a third channel in a spaceborne lidar would bring. Future work will consist to adapt this retrieval scheme to accurate radiative transfer models and apply it to actual aircraft and satellite data. Further constraints to the retrieval could be achieved by including other sources of observations such as POLDER which could help to better characterize fine-mode aerosol models [*Herman et al.*, 2005] and thus improve the retrieval for the case of predominance of coarse-mode aerosols.

[42] **Acknowledgments.** This work forms part of NH PhD, which is supported by the Centre National d'Etudes Spatiales (CNES) and the Region Nord-Pas-de-Calais. OB was supported by the Climate Prediction Programme of the UK Department for Environment, Food, and Rural Affairs and the GEMS project of the European Commission. The authors are grateful to Frédéric Chevallier, Angela Benedetti, and Laurent Labonotte for their useful comments. Laurent Hascoët and the TROPICS team are acknowledged for their technical assistance in automatic differentiation. TAPENADE can be downloaded from http://www-sop.inria.fr/tropics/tapenade.html. The authors would like to pay tribute to Yoram Kaufman whose huge contribution to satellite aerosol retrieval has formed the background for this study.

References

Ackerman, S., O. B. Toon, D. E. Stevens, A. J. Heymsfield, V. Ramanathan, and E. J. Welton (2000), Reduction of tropical cloudiness by soot, *Science*, *288*, 1042–1047.

Anderson, T. L., et al. (2005), A-Train strategy for quantifying direct climate forcing by aerosols, *Bull. Am. Meteorol. Soc.*, *86*(12), 1795–1809.

Bellouin, N., O. Boucher, J. Haywood, and M. S. Reddy (2005), Global estimate of aerosol direct radiative forcing from satellite measurements, *Nature*, *438*, 1138–1141.

Byrd, R. H., P. Lu, J. Nocedal, and C. Zhou (1994), A limited memory algorithm for bound constrained optimization, in *Technical report NAM-08*, Northwestern University, Evanston, USA.

Chazette, P. (2003), The monsoon aerosol extinction properties at Goa during INDOEX as measured with Lidar, *J. Geophys. Res.*, *108*(D6), 4187, doi:10.1029/2002JD002074.

Collins, W. D., P. J. Rasch, B. E. Eaton, B. V. Khattatov, J.-F. Lamarque, and C. S. Zender (2001), Simulating aerosols using a chemical transport model with assimilation of satellite aerosol retrievals: Methodology for INDOEX, *J. Geophys. Res.*, *106*, 7313–7336.

Deuzé, J.-L., P. Goloub, M. Herman, A. Marchand, G. Perry, S. Susana, and D. Tanré (2000), Estimate of the aerosol properties over ocean with POLDER, *J. Geophys. Res.*, *105*, 15,329–15,346.

Deuzé, J.-L., et al. (2001), Remote sensing of aerosols over land surfaces from POLDER-ADEOS-1 polarized measurements, *J. Geophys. Res.*, *106*, 4913–4926.

Hascoët, L., and V. Pascual (2004), TAPENADE 2.1 User's guide, in *Technical report*, Sophia-Antipolis, France. (http://www-sop.inria.fr/tropics)

Herman, M., J.-L. Deuzé, A. Marchand, B. Roger, and P. Lallart (2005), Aerosol remote sensing from POLDER/ADEOS over the ocean: Improved retrieval using a nonspherical particle model, *J. Geophys. Res.*, *110*, D10S02, doi:10.1029/2004JD004798.

Janiskova, M., and J.-J. Morcrette (2005), Investigation of the sensitivity of the ECMWF radiation scheme to input parameters using adjoint technique, *Q. J. R. Meteorol. Soc.*, *131*, 1975–1996.

Kaufman, Y. J., D. Tanré, J. F. Léon, and J. Pelon (2003), Retrievals of fine and coarse aerosols using lidar and radiometric space measurements, *IEEE Trans. Geosci. Remote Sens.*, *41*, 1743–1754.

Kaufman, Y. J., O. Boucher, D. Tanré, M. Chin, L. A. Remer, and T. Takemura (2005), Aerosol anthropogenic component estimated from satellite data, *Geophys. Res. Lett.*, *32*, L17804, doi:10.1029/2005GL023125.

Le Dimet, F. X., and O. Talagrand (1986), Variational algorithms for analysis and assimilation of meteorological observations: Theoretical aspects, *Tellus*, *38A*, 97–110.

Léon, J.-F., D. Tanré, J. Pelon, Y. J. Kaufman, J. M. Haywood, and B. Chatenet (2003), Profiling of a Saharan dust outbreak based on a synergy between active and passive remote sensing, *J. Geophys. Res.*, *108*(D18), 8575, doi:10.1029/2002JD002774.

Marks, C., and C. Rodgers (1993), A retrieval method for atmospheric composition from limb emission measurement, *J. Geophys. Res.*, *98*, 14,939–14,953.

Menon, S., J. Hansen, L. Nazarenko, and Y. Luo (2002), Climate effects of black carbon aerosols in China and India, *Science*, *297*, 2250–2253.

Miura, T., A. R. Huete, and H. Yoshioka (2000), Evaluation of sensor calibration uncertainties on vegetation indices for MODIS, *IEEE Trans. Geosci. Remote Sens.*, *38*(3), 1399–1409.

Müller, D., K. Franke, F. Wagner, D. Althausen, A. Ansmann, and J. Heintzenberg (2001), Vertical profiling of optical and physical particle properties over the tropical Indian Ocean with six-wavelength lidar: 2. Case studies, *J. Geophys. Res.*, *106*(D22), 28,577–28,595.

Reddy, M. S., O. Boucher, N. Bellouin, M. Schulz, Y. Balkanski, J.-L. Dufresne, and M. Pham (2005), Estimates of global multicomponent aerosol optical depth and direct radiative perturbation in the Laboratoire de Météorologie Dynamique general circulation model, *J. Geophys. Res.*, *110*, D10S16, doi:10.1029/2004JD004757.

Remer, L. A., et al. (2005), The MODIS aerosol algorithm, products and validation, *J. Atmos. Sci.*, *62*, 947–973.

Rosenfeld, D. (2000), Suppression of rain and snow by urban and industrial air pollution, *Science*, *287*, 1793–1796.

Rosenfeld, D., R. Lahav, A. P. Khain, and M. Pinsky (2002), The role of sea spray in cleansing air pollution over ocean via cloud processes, *Science*, *297*, 1667–1670.

Stephens, G. L., R. J. Engelen, M. Vaughan, and T. L. Anderson (2001), Toward retrieving properties of the tenuous atmosphere using space-based lidar measurements, *J. Geophys. Res.*, *106*, 28,143–28,157.

Yu, H., et al. (2006), A review of measurement-based assessment of aerosol direct radiative effect and forcing, *Atmos. Chem. Phys.*, *6*, 613–666.

O. Boucher, Hadley Centre, Met Office, Exeter, United Kingdom. (olivier.boucher@metoffice.gov.uk)

N. Huneeus, Laboratoire d'Optique Atmosphérique, Centre National de la Recherche Scientifique/Université des Sciences et Technologies de Lille, Villeneuve d'Ascq, France. (huneeus@loa630.univ-lille1.fr)